Epithelial control of colonisation by *Streptococcus pneumoniae* at the human mucosal surface

Caroline M Weight[1], Cristina Venturini[1], Sherin Pojar[2], Simon P. Jochems[2], Jesús Reiné[2], Elissavet Nikolaou[2], Carla Solórzano[2], Mahdad Noursadeghi[1], Jeremy S Brown[3], Daniela M. Ferreira[2], Robert S Heyderman[1]

[1]Division of Infection and Immunity, University College London, London, United Kingdom, [2]Department of Clinical Sciences, Liverpool School of Tropical Medicine, Liverpool, United Kingdom, [3]Department of Respiratory Medicine, University College London, London, United Kingdom

Corresponding Author: Dr Caroline M. Weight, Division of Infection and Immunity, The Rayne Building, 5 University Street, University College London, WC1E 6JF, UK.

Email: c.weight@ucl.ac.uk; Tel: +44 20 3108 2351

ABSTRACT

Control of *Streptococcus pneumoniae* colonisation at human mucosal surfaces is critical to reducing the burden of pneumonia and invasive pneumococcal disease, interrupting transmission, and achieving herd protection. Using an Experimental Human Pneumococcal Carriage Model (EHPC), we show that *S. pneumoniae* colonisation is associated with epithelial surface adherence, microcolony formation and invasion, without overt disease. The finding of co-association with junctional proteins provides a possible mechanism for this so-called micro-invasion. Using epithelial modules from a human epithelial cell model that recapitulates our *in vivo* findings, comprising innate signalling/ regulatory pathways, inflammatory mediators, cellular metabolism and stress response genes, we find that inflammation in the EHPC model is most prominent around the time of bacterial clearance. These results show that rather than being confined to the epithelial surface and the overlying mucus layer, the pneumococcus undergoes micro-invasion which enhances the inflammatory/ innate immune response associated with clearance which may also trigger transmission.

Introduction

Colonisation of upper respiratory tract (URT) mucosa by a range of pathogenic bacteria is a necessary precursor to both disease and onward transmission. *Streptococcus pneumoniae*, also known as pneumococcus, is a common coloniser of the human nasopharynx but is also estimated to be responsible for >500,000 deaths due to pneumonia, meningitis and sepsis in children under five years of age worldwide[1]. In comparison to gut pathogen-mucosal interactions[2], the control of pneumococcal URT colonisation is far less well understood, particularly in humans[3].

In Europe and North America, there has been a dramatic effect of pneumococcal conjugate vaccine (PCV) on vaccine serotype (VT) invasive disease and carriage[4,5]. Indeed, more than 50% of PCV impact has been attributed to a reduction in VT colonisation resulting in reduced transmission and therefore disease, so-called herd protection[4,5]. However, the emergence of non-VT pneumococcal disease across the world and the more modest impact of PCV on colonisation in high transmission settings threaten this success[6-10]. Defining the mechanistic basis for host control of pneumococcal colonisation at the mucosal surface is therefore crucial for the further optimisation of therapeutic interventions which target carriage and transmission.

We and others have previously shown that in humans, URT mucosal T cell immune memory specific to subcapsular pneumococcal protein antigens is acquired with age and predominately pro-inflammatory, but heavily controlled by Treg[11-13]. In contrast to PCV-induced protection, this naturally acquired protective immunity is thought to also comprise antibodies to protein antigens which have been implicated in the prevention of colonisation and the mediation of clearance[14]. The URT epithelium is at the centre of this process[15,16] through the binding and transporting of antibodies, sensing bacteria colonising the mucosal surface via a range of surface and intracellular pathogen-associated molecular patterns (PAMPs) receptors, and rapidly transducing signals to recruit both innate, inflammatory and adaptive immune mechanisms[17-19].

77 Murine models of colonisation and invasion suggest that adherence of *S. pneumoniae* to the mucosal
78 epithelium may be followed by paracellular transmigration and tight junction modulation[20-22]. In
79 contrast, studies of immortalised epithelial cell monolayers implicate endocytosis of *S. pneumoniae*,
80 mediated though pneumococcal protein C–polymeric immunoglobulin receptor interactions[23,24]. The
81 relative importance of epithelial endocytosis and paracellular migration in colonisation and invasion
82 remains uncertain[24], but may influence epithelial sensing of this otherwise extracellular pathogen.
83 This may include TLR2 signalling via lipoteichoic acid[25,26], Nod1 signalling via peptidoglycan[27] and
84 TLR4 signalling via pneumolysin[28,29], a pore-forming toxin that mediates both clearance and
85 transmission in an infant mouse model[28-30].

86

87 We have therefore explored the hypothesis that pneumococcal-epithelial engagement dictates the
88 inflammatory/ innate immune response and therefore the outcome of colonisation. Much of what we
89 understand of the control of pneumococcal colonisation is derived from epidemiological studies and
90 murine carriage models. The experimental human pneumococcal carriage (EHPC) model provides
91 a well-controlled, reproducible tool to characterise the cellular and molecular mechanisms that
92 underlie pneumococcal colonisation in humans[31]. We have used human epithelial cell lines to further
93 probe these mechanisms and derive epithelial transcriptome module to interrogate the host response
94 in the EHPC model. Here, we show that pneumococcal colonisation in humans is characterised by
95 microcolony formation, junctional protein association (Junctional Adhesion Molecule A (JAM-A) and
96 β-catenin) and migration across the epithelial barrier without disease, which we have termed micro-
97 invasion. This pattern of bacterial-host cell association shapes epithelial sensing of *S. pneumoniae*
98 which is partially pneumolysin dependent. Together, our data suggest that the epithelial barrier is
99 breached in the early phases of pneumococcal colonisation, and that this may occur without eliciting
100 a marked host response. As colonisation becomes more established, epithelial sensing of *S.*
101 *pneumoniae* enhances innate immunity/ inflammation which we propose promotes clearance and
102 may also trigger transmission.

103

104

105 **RESULTS**

106 **Pneumococcal colonisation of the human nasopharynx is associated with epithelial**
107 **adhesion, microcolony formation and micro-invasion**

108 We have used an EHPC model[32] to capture the epithelial events central to pneumococcal
109 colonisation, obtaining human mucosal samples by curette biopsy. We defined a carrier as an
110 individual colonised by 6B *S. pneumoniae* as detected by culture of nasal wash at any day following
111 inoculation (days 2, 6, 9, 14 - 27). Clearance was defined as when *S. pneumoniae* colonisation
112 became negative by culture of nasal wash.

113

114 Colonisation was detected in 9/13 healthy volunteers by culture, 12/13 by microscopy and 9/11 by
115 LytA PCR (Table 1). Carriage was detected by culture/ PCR at day 2, whereas maximum detection
116 by microscopy was evident at day 6. This is not explained by colonisation density and therefore the
117 sensitivity of culture/ PCR. This could be explained by greater association with the epithelium
118 (detected by all techniques) rather than the overlying mucus (detected by culture/PCR but not
119 microscopy) over time. Clearance generally occurred between day 9 and day 27 (Table 1 and Figure
120 1b).

121

122 Curette biopsy samples visualised by confocal microscopy using Wheat Germ Agglutinin (WGA) as
123 a marker for surface carbohydrates and JAM-A as a marker of tight junctions, yielded intact sheets
124 of epithelial cells associated with polymorphonuclear leukocytes, characterised morphologically
125 (Figure 1a and Supplementary Figure 1a). Amongst carriers, pneumococci were found on the
126 epithelial surface (Table 1; Figure 1c, Figure 1d) which over time became associated with
127 microcolony formation (Figure 1e). There was also evidence of pneumococcal invasion of the
128 epithelial monolayer without disease which we have termed “micro-invasion” (Figure 1e-f).
129 Pneumococci were also observed in phagocytic cells (Supplementary Figure 1a). Colonisation was
130 frequently characterised by co-association between *S. pneumoniae* and JAM-A (Figure 1f). This
131 intimate association between inoculated pneumococci and the mucosa in the EHPC model is

132 suggestive of an active process that reflects natural asymptomatic pneumococcal carriage in
133 humans.
134
135 **Epithelial surface marker expression *in vivo* is not altered in response to colonisation with *S.***
136 ***pneumoniae***
137 To determine whether pneumococcal colonisation leads to epithelial activation, we stained nasal
138 curette biopsy cell suspensions for surface expression of EpCAM (epithelial cell identification), IL-
139 22Ra1, HLADR, CD40, CD54 and CD107a prior to analysis by flow cytometry (Supplementary
140 Figure 2a-d). We did not detect a significant change in the relative expression of IL-22Ra1 (protects
141 the epithelial barrier, promotes anti-microbial product secretion during infection, modulating
142 pneumococcal carriage and clearance [33-36]), HLADR (mediates T cell-antigen recognition and is a
143 marker of epithelial activation[37]), CD40 (co-stimulatory protein which binds CD154[38] (Supplementary
144 Figure 2e-g) or CD54 (a leukocyte adhesion molecule which is also upregulated by CD40[38-40],
145 initiating neutrophil migration and recruitment[41,42]) (Figure 1g). However, although the number of
146 epithelial cells expressing CD107a did not change over time (Figure 1h), we did observe an increase
147 in CD107a^{high} expression at day 2 post inoculation in carriage positive volunteers vs. carriage
148 negative volunteers (Figure 1h). CD107a is also known as lysosomal associated membrane protein
149 1 (LAMP-1), which in the epithelium forms the membrane glycoprotein of late endosomes and
150 phagolysosomes and endosomes[24] and has previously been implicated in pneumococcal
151 endocytosis[24]. These data highlight the ability of the pneumococcus to colonise the nasopharynx
152 without marked inflammation and potentially implicate CD107a in the process.
153
154 ***S. pneumoniae* infection of nasopharyngeal epithelial cells *in vitro* is associated with**
155 **pneumococcal adhesion, microcolony formation and micro-invasion**
156 To further understand the epithelial responses to *S. pneumoniae* adherence and micro-invasion
157 observed in the EHPC model, we undertook infection experiments with Detroit 562 epithelial cells
158 (nasopharyngeal carcinoma derived). We compared the 6B response with two other representative
159 clinical isolates, TIGR4 (the original sequenced strain[43]) and 23F, and a TIGR4 pneumolysin deletion

160 mutant strain (dPly). Pneumolysin is a key pore-forming virulence factor that induces
161 inflammation[15,29].

162

163 TIGR4 association (adherence and invasion as detected by culture) with Detroit 562 cells was over
164 100-fold higher for adhesion and over 70-fold higher for invasion after three hours infection,
165 compared to 6B or 23F strains (Figure 2a-b). Using confocal microscopy to identify the nature of this
166 association (Figure 2d-e, and Supplementary Figure 3a), pneumococcal adhesion to the epithelial
167 surface was found associated with microcolony formation and also internalisation of this
168 conventionally extracellular pathogen[22] (Figure 2d-e, Supplementary Figure 3a). Intracellular
169 pneumococci were contained within intracellular vesicles suggestive of endocytosis, which was most
170 marked with the TIGR4 strain (Figure 2b)[24]. Intracellular pneumococci were coated with JAM-A
171 (Figure 2f, Supplementary Figure 3a) and associated with the adherens junction protein β catenin
172 but not Claudin 4 (Supplementary Figure 3a). Laterally located pneumococci were identified
173 transiting between cell junctions (Figure 2g), located at the level of the nuclei and below the basal
174 membrane (Figure 2h). Transmigration across the epithelium (endocytosis or paracellular
175 movement), as measured by the culture of pneumococci from the basal chamber of transwell inserts,
176 was most marked with 23F (Figure 2c, five-fold higher compared to TIGR4, after three hours
177 infection). In each of these experiments a similar pattern of epithelial interaction was seen at one
178 hour suggesting that these observations are not simply explained by differential growth during
179 colonisation.

180

181 Epithelial infection with the dPly TIGR4 mutant showed a significant increase in association (Figure
182 2a, ten-fold higher after three hours infection), internalisation (Figure 2b, three-fold higher after three
183 hours infection), but no significant differences in transmigration (Figure 2c) compared to the wild-
184 type strain, implicating pneumolysin in the modulation of bacterial interactions with the epithelium.

185

186 Similar patterns of adherence and invasion were observed in infection experiments with human
187 bronchial carcinoma Calu3 epithelial cells and human alveolar epithelial carcinoma A549 epithelial
188 cell lines demonstrating that these findings are not cell-line dependent (Supplementary Figure 4).
189 Furthermore, primary epithelial cells from curette biopsies were differentiated on an air-liquid
190 interface for 30 days and co-cultured with either 6B or 23F *S. pneumoniae*. Pneumococcal
191 microcolony formation, micro-invasion and epithelial junctional protein association were also
192 observed with these long-term primary nasal epithelial cells (Supplementary Figure 1b).

193

194 Together these data show the strain dependency of pneumococcal-epithelial interactions *in vitro*
195 which mirror the pathways for epithelial micro-invasion seen *in vivo*.

196

197 **Endocytosis-related micro-invasion and transmigration**

198 To confirm that the pneumococcal endocytosis observed by confocal microscopy leads to
199 transmigration across the epithelium, endocytosis was inhibited with dynasore and nystatin[24]. After
200 one hour of infection, cellular uptake of 23F was inhibited by 82% (Figure 2i) and transmigration
201 across the cell monolayer by 85% (Figure 2j). This inhibition of endocytosis and transmigration was
202 also seen with TIGR4 (data not shown). In agreement with previous studies using A549 and Calu3
203 cells[44], we found that viable pneumococci in Detroit 562 cells decreased over time (Supplementary
204 Figure 5a). Using gentamicin treatment to eliminate the original extracellular inoculum, we have
205 observed *S. pneumoniae* in the apical and basal media (Supplementary Figure 5b), suggesting
206 egress from the epithelium.

207

208 **Loss of epithelial cell barrier function is not a pre-requisite for micro-invasion by *S.***
209 ***pneumoniae***

210 *S. pneumoniae* has been shown to affect the integrity of epithelial barriers and tight junction function
211 in murine models[21,45]. Having demonstrated pneumococcal micro-invasion in the EHPC model and

212 in epithelial cells *in vitro* without obvious epithelial morphological disruption, we have explored the
213 possibility that pneumococcal micro-invasion, particularly paracellular transmigration, may occur
214 without disruption of epithelial barrier function. As it was not possible to directly assess epithelial
215 barrier function in the EHPC model, we have measured trans-epithelial electrical resistance (TEER)
216 and permeability as assessed by 4kDa FITC-dextran in Detroit 562 cells. TEER was not adversely
217 affected by pneumococcal co-culture (Figure 2k) and permeability was maintained with all the
218 pneumococcal strains (Figure 2l). Although co-localisation of pneumococci was seen with host
219 proteins, we did not detect marked epithelial membrane carbohydrate or protein re-distribution
220 (WGA, Claudin 4 JAM-A, β catenin, Supplementary Figure 3a). Similar observations were made with
221 A549 cells and Calu3 cells (Supplementary Figure 4). These data suggest that pneumococcal micro-
222 invasion is not dependent on loss of epithelial cell barrier function during early interactions.

223

224 ***S. pneumoniae* upregulates epithelial surface CD54 and CD107a *in vitro***

225 To further explore the possibility that the epithelial surface marker expression seen in the 6B EHPC
226 model reflects the pattern of epithelial adhesion and micro-invasion, we assessed Detroit 562 cell
227 surface marker expression in response to our *S. pneumoniae* panel as before (Supplementary Figure
228 7a-c). There were no significant changes in IL-22Ra1, HLADR or CD40 expression in response to
229 6B, 23F, TIGR4 and dPly strains (Supplementary Figure 7d-e). However, $CD54^{high}$ expression was
230 significantly greater in response to the TIGR4 and dPly strains, compared to non-infected cells
231 (Figure 3a). Epithelial CD107a was upregulated in response to the 6B, 23F and TIGR4 strains
232 (Figure 3b), but this was not seen with the dPly mutant. These data implicate pneumolysin in the
233 induction of CD107a but not CD54 epithelial surface expression, and support the possibility that
234 CD107a is involved in pneumococcal-epithelial micro-invasion events seen *in vivo*.

235

236 ***Streptococcus pneumoniae* induces epithelial secretion of IL-6, IL-8 and CD54**

237 To further assess the inflammatory consequences of the pneumococcal-epithelial infection *in vitro*,
238 we measured a panel of cytokines in the supernatants of Detroit 562 cells following incubation with

239 *S. pneumoniae* (Figure 3c). We detected a significant increase in IL-6 and IL-8, which were strain-
240 dependent and partially pneumolysin dependent. In line with the surface marker observations, only
241 TIGR4 significantly upregulated the secretion of soluble CD54, which was again dependent on the
242 presence of pneumolysin in this strain (Figure 3c). These data highlight the less inflammatory nature
243 of the 6B strain used in the EHPC model compared to the more invasive strain, TIGR4 and the
244 importance of pneumolysin in the epithelial response. Pneumococcal wild-type strain differences are
245 not explained by differences in pneumolysin activity, as determined by hemolysis (Supplementary
246 Figure 7).

247

248 **Innate transcriptomic response to epithelial infection by *S. pneumoniae in vitro***

249 To further explore the hypothesis that the pattern of epithelial adhesion and micro-invasion results
250 in differential epithelial responses, we performed RNAseq of Detroit 562 cells infected with our panel
251 of *S. pneumoniae* strains for 3 hours. In comparison to non-infected epithelial cell cultures (Figure
252 4a), infection with TIGR4 upregulated expression of 1127 genes (550 unique genes), 23F
253 upregulated 650 genes (69 unique genes), and 6B upregulated 153 genes (10 unique genes). The
254 pneumolysin deficient isogenic mutant of TIGR4 upregulated 220 genes (14 unique genes).
255 Compared to non-infected cells, 1193 genes were upregulated by *S. pneumoniae* infection overall
256 and 93 were core to all the strains tested. The sets of genes upregulated by each strain individually
257 were subjected to core and interactome and pathway enrichment analysis for functional annotation
258 of the cellular response at systems level (Figure 4b, Online Supplementary File). From 20 clusters
259 of pathways, the pathway consisting of the largest total number of genes was selected to provide a
260 representative annotation for each cluster (Figure 4c and Supplementary Figure 8). Significant
261 enrichment of innate immune system responses was evident in all strains and included specific
262 enrichment in Toll receptor cascades, peptide ligand-binding receptors, NFkB and MAP kinase
263 activation, Interferon signalling and cytokine and chemokine signalling, (Figure 4b, 4c). In general,
264 the greater number of transcripts upregulated by TIGR4 and 23F strains compared to 6B translated
265 to a larger number of biological pathways with differential innate immune responses to each strain
266 (Figure 4b). Fewer transcriptional responses at the level of functional pathways in response to the

267 pneumolysin deficient mutant of TIGR4 is consistent with a role for pneumolysin in innate immune
268 recognition of *S. pneumoniae* previously reported in macrophages[46]. Fewer transcriptional
269 responses to 6B is consistent with our observations that this strain is associated with the lowest level
270 of cellular association and transmigration.

271

272 To further explore the pathways that drive the transcriptional responses to each strain, we also
273 undertook transcription factor binding site enrichment analysis (Figure 4d, Online Supplementary
274 File). The responses to 6B and pneumolysin deficient strains were principally enriched in binding
275 sites for the NFkB/Rel family of transcription factors, indicating that an NFkB activation pathway was
276 the dominant driver for the responses to these strains. In contrast, cellular responses to TIGR4 and
277 23F strains revealed enriched binding sites for more diverse transcription factors, suggesting diverse
278 molecular pathways by which these strains may influence cellular function. This analysis revealed
279 particular enrichment of binding sites for beta-beta-alpha zinc finger superfamily of transcription
280 factors, including SP1 and KLF4, suggesting that these strains upregulate mitogen activated protein
281 kinase pathways upstream of these transcription factors[47].

282

283 **Epithelial transcriptomic responses to 6B are detectable *in vivo***

284 Next, we sought to test whether these epithelial transcriptomic responses to *S. pneumoniae* were
285 also evident in the 6B EHPC model. We compared nasal transcriptomes sampled at two or nine days
286 after inoculation to pre-inoculation samples. These revealed significant enrichment of 158 transcripts
287 among individuals who became colonised (Supplementary Figure 9). These genes included Claudin
288 5 and Claudin 17; Defensin β 103A/B, Cadherin 16, Desmocollin 1 and Gap junction protein α1,
289 which suggests cytoskeletal re-organisation two days post-inoculation in carriage positive
290 individuals. At day 9 post-inoculation, innate molecules such as CCR3, matrix metalloproteinase 12
291 and MHC II molecules are enriched, suggesting innate activation. However, these gene sets were
292 not significantly enriched for any immune response pathway annotation perhaps because of the

293 statistical stringency necessary for genome-wide multiple testing, and were not epithelial specific
294 responses.

295

296 Gene expression modules have been used successfully to detect specific transcriptional programs
297 in bulk tissue[48-50]. Therefore, as an alternative approach, we sought to target specific epithelial
298 responses *in vivo* using the *in vitro* interactome. A direct comparison of transcripts for 6B revealed
299 FOSL-1, an AP-1 transcription factor subunit, to be enriched with carriage. To expand the sensitivity
300 of the approach, we evaluated the expression of two transcriptional modules in the nasal samples
301 (Figure 5). A 'core' module comprised of 16 interacting genes (Figure 5b) that were upregulated in
302 the Detroit epithelial cells by all the pneumococcal strains from Figure 5a, and a second 'integrated'
303 module that comprised of 200 interacting genes (Figure 5c) which were upregulated in the Detroit
304 epithelial cells by at least one of the pneumococcal strains from Figure 5a. Among the individuals
305 who failed to become colonised by the bacterial challenge, we found no increase in expression in
306 either gene expression modules (Figure 5b-c). In contrast among the individuals who became
307 colonised, the expression of both modules but significantly increased within the integrated module
308 at day nine (Figure 5b,5c). The prominence of this response at day nine may reflect time-dependent
309 proliferation of the 6B bacterial inoculum and the subsequent epithelial interactions. This response
310 was apparent around the time of the subsequent clearance of these bacteria.

311

312 **DISCUSSION**

313 It is widely accepted that colonisation of the upper respiratory tract mucosa by many potentially
314 pathogenic bacterial species, involves transient association with the overlying mucus layer but
315 adherence to the epithelial surface avoids mucus entrapment and muco-ciliary clearance[22,51]. While
316 evading immunity, bacterial replication then occurs prior to onward transmission to a new host. Even
317 for *S. pneumoniae,* one of the most common infectious causes of human life-threatening disease,
318 the mechanisms underlying this transition from acquisition to established colonisation, and then
319 transmission and/or disease, are not well understood. By combining an EHPC model and *in vitro*

320 human cell culture systems, we show that pneumococcal colonisation leads to epithelial adherence,
321 microcolony formation and migration across the epithelial barrier without disease, which we have
322 termed micro-invasion. The finding of co-association with junctional proteins provides a possible
323 mechanism for micro-invasion. We also demonstrate that the innate epithelial response to
324 pneumococcal colonisation is dependent on the pattern of bacterial-host cell association. Indeed,
325 epithelial micro-invasion and not bacterial load *per s*e, appears to dictate unique transcription factor
326 binding site signatures, and downstream cytokine, chemokine and metabolic pathway enrichment
327 (Figure 6).

328

329 The concept of mucosal micro-invasion without overt disease moves us away from current models
330 of colonisation in which the pneumococcus is held up at the epithelial surface. Our data are
331 supported by murine colonisation experiments[52,53] and the detection of pneumococcal DNA in the
332 blood of otherwise healthy colonised children[54]. Using primary and immortalised epithelial cell line
333 models that mirror this process, and in line with other cell culture and murine models[45,52,55,56], we
334 have demonstrated that pneumococcal micro-invasion occurs by endocytosis through the formation
335 of cytoplasmic vacuoles, and by paracellular transcytosis across the epithelium. Micro-invasion of
336 the epithelium may overcome the inaccessibility of PAMP receptors located either at the epithelial
337 basolateral surface or intracellularly[57-59]. We have found that micro-invasion *in vitro* is also
338 characterised by pneumococcal co-association with JAM-A and β catenin, without evidence of
339 barrier dysfunction at early time points. In murine models at later time points, TLR-dependent Claudin
340 7 and Claudin 10 down-regulation and disruption of multiple junctional proteins in human lung tissue,
341 that enhanced pneumococcal translocation across the epithelium, has been observed[21,45]. While this
342 may occur as inflammation becomes more prominent, our data suggest that microinvasion can
343 happen without epithelial barrier disruption and that the epithelium plays an active role in the
344 regulation of these complex host-pathogen interactions[19,60,61].

345

346 The differential impact of micro-invasion on the epithelial transcriptomic response was striking with
347 considerable enrichment of multiple diverse transcription factors and signalling pathways related to
348 innate immunity with the most invasive pneumococcal strains. The interactome module highlights
349 that although enrichment of gene activation in response to all pneumococcal strains is apparent (the
350 core module), a more diverse range of epithelial gene activation occurs between strains, reflecting
351 specific host-pathogen interactions. Nasal colonisation in murine models is proinflammatory[20,62], but
352 our *in vitro* and EHPC experiments with serotype 6B suggest that this is not always the case,
353 whereby pneumococcal-host cell adherence, growth, endocytosis and paracellular migration can be
354 established in the absence of a marked host response. In the EHPC, clearance occurred around the
355 time that the epithelial transcriptomic response was most prominent. Weiser and colleagues have
356 long made the case that the colonising pneumococcus induces the host response that mediates
357 clearance, but also promotes nutrient acquisition and transmission[22,63]. This is supported by murine
358 models[64] and epidemiological studies of viral-coinfection[65,66] that suggest that the host response to
359 pneumococcal colonisation promotes onward transmission to susceptible individuals.[29] The
360 enrichment of binding sites for SP1 and KLF4 transcription factors seen in our *in vitro* data suggest
361 that there may be a counter-regulatory process aimed at minimising inflammation. KLF4 plays a role
362 in barrier function, suppression of NFκB-dependent IL-8 secretion, regulation of IL-10 expression via
363 TLR9-MyD88 and Yes-1, in response to *S. pneumoniae,* which is partially dependent on the autolysin
364 LytA[47,67,68]. Thus, by exploiting micro-invasion, the pneumococcus may carefully calibrate the host
365 innate immune/ inflammatory response to promote survival through transmission.
366

367 A range of pneumococcal PAMPs including pneumolysin, may trigger this epithelial sensing
368 process[29,69]. We found pneumolysin to be a prominent trigger of epithelial surface molecule
369 upregulation, cytokine production and the transcriptomic inflammatory response *in vitro*. Mediated
370 by autolysin, the pneumococcus undergoes autolysis when reaching stationery growth phase,
371 resulting in the release of additional PAMPs including bacterial DNA. In mice, pneumococcal DNA
372 triggers inflammation through a DAI/STING/TBK1/IRF3 cascade[62,70], a response that may also
373 contribute to pneumococcal clearance. We detected enriched activation of IRF3/IFR7 in the TIGR4

374 pneumolysin deficient strain in our *in vitro* transcriptomic analyses. Whether induction of type 1
375 interferons by host or bacterial RNA during human pneumococcal infection mediates bacterial
376 clearance by the epithelium remains to be determined. We therefore suggest that in the context of
377 micro-invasion, pneumococcal DNA may act as a trigger of epithelial sensing, inducing inflammation
378 and that cellular entry of DNA may be enhanced by pneumolysin pore formation[70].

379

380 Our findings are limited by the pneumococcal strains available for testing in the EHPC model to
381 enable direct comparisons between the *in vivo* and *in vitro* data. Nonetheless, the use of different
382 strains *in vitro* has enabled us and others[56,71] to determine the impact of different patterns of epithelial
383 adherence and invasion on the host inflammatory/ innate immune response. Although, our
384 observations have been based on immortalised cell lines, the findings are supported by studies of
385 primary cell lines *ex vivo* in an air-liquid interface derived from the EHPC and by the EHPC itself.

386

387 In conclusion, our data implicates the novel finding micro-invasion in pneumococcal colonisation of
388 otherwise healthy humans. Micro-invasion may influence the outcome of colonisation by altering the
389 balance between innate immunity/ inflammation-driven transmission and clearance. This balance
390 may be further modulated by the frequency of carriage events, pneumococcal strain co-colonisation,
391 viral co-infections and other environmental pressures[1,64,72]. The pathways critical for onward
392 pneumococcal transmission remain to be determined in humans. Our approach combining *in vitro*
393 and *in vivo* human systems offers a potentially tractable way to interrogate this question.

394

395

396 **ACKNOWLEDGEMENTS**

397 This study was funded by the Wellcome Trust (Grant 106846/Z/15/Z). DF is supported by the Medical
398 Research Council (grant MR/M011569/1), Bill and Melinda Gates Foundation (grant OPP1117728)
399 and the National Institute for Health Research (NIHR) Local Comprehensive Research Network.
400 LytA PCR was performed by Prof. D Bogaert, University of Edinburgh, UK. RNAseq library

401 preparation undertaken at either UCL through the Pathogens Genomic Unit or at the Wellcome
402 Sanger Institute, Hinxton with thanks to Carl Anderson. Confocal imaging facilities at LSTM were
403 funded by a Wellcome Trust Multi-User Equipment Grant (104936/Z/14/Z). Flow cytometric
404 acquisition was funded by a Wellcome Trust Multi-User Equipment Grant (104936/Z/14/Z).

405

406 **AUTHOR CONTRIBUTIONS**: CMW, SPJ, DMF and RSH conceived and designed the study. CMW,
407 SP, SPJ, JR, EN, CS acquired the data. CMW, CV, SPJ, MN, JSB, DMF, RSH analysed and
408 interpreted the data. CMW wrote the first draft of the manuscript. CMW, CV, SP, SPJ, JR, EN, CS,
409 MN, JSB, DMF, RSH commented on and approved the manuscript.

410

411 **COMPETING INTERESTS:** The authors declare no competing financial interests.

412

413 **REFERENCES**

414
415

416 1. O'Brien, K.L.*, et al.* Burden of disease caused by Streptococcus pneumoniae in children younger than
417 5 years: global estimates. *Lancet* **374**, 893-902 (2009).
418 2. Kagnoff, M.F. The intestinal epithelium is an integral component of a communications network. *J Clin*
419 *Invest* **124**, 2841-2843 (2014).
420 3. Jochems, S.P., Weiser, J.N., Malley, R. & Ferreira, D.M. The immunological mechanisms that control
421 pneumococcal carriage. *PLoS Pathog* **13**, e1006665 (2017).
422 4. Shiri, T.*, et al.* Indirect effects of childhood pneumococcal conjugate vaccination on invasive
423 pneumococcal disease: a systematic review and meta-analysis. *Lancet Glob Health* **5**, e51-e59 (2017).
424 5. Whitney, C.G.*, et al.* Decline in invasive pneumococcal disease after the introduction of protein-
425 polysaccharide conjugate vaccine. *N Engl J Med* **348**, 1737-1746 (2003).
426 6. Usuf, E., Bottomley, C., Adegbola, R.A. & Hall, A. Pneumococcal carriage in sub-Saharan Africa--a
427 systematic review. *PLoS One* **9**, e85001 (2014).
428 7. Brueggemann, A.B., Pai, R., Crook, D.W. & Beall, B. Vaccine escape recombinants emerge after
429 pneumococcal vaccination in the United States. *PLoS Pathog* **3**, e168 (2007).
430 8. Hanage, W.P.*, et al.* Carried pneumococci in Massachusetts children: the contribution of clonal
431 expansion and serotype switching. *Pediatr Infect Dis J* **30**, 302-308 (2011).
432 9. Pillai, D.R.*, et al.* Genome-wide dissection of globally emergent multi-drug resistant serotype 19A
433 Streptococcus pneumoniae. *BMC Genomics* **10**, 642 (2009).
434 10. Mosser, J.F.*, et al.* Nasopharyngeal carriage and transmission of Streptococcus pneumoniae in
435 American Indian households after a decade of pneumococcal conjugate vaccine use. *PLoS One* **9**,
436 e79578 (2014).
437 11. Pido-Lopez, J., Kwok, W.W., Mitchell, T.J., Heyderman, R.S. & Williams, N.A. Acquisition of
438 pneumococci specific effector and regulatory Cd4+ T cells localising within human upper respiratory-
439 tract mucosal lymphoid tissue. *PLoS Pathog* **7**, e1002396 (2011).
440 12. Glennie, S.J.*, et al.* Regulation of naturally acquired mucosal immunity to Streptococcus pneumoniae
441 in healthy Malawian adults and children. *PLoS One* **7**, e51425 (2012).
442 13. Zhang, Q.*, et al.* Characterisation of regulatory T cells in nasal associated lymphoid tissue in children:
443 relationships with pneumococcal colonization. *PLoS Pathog* **7**, e1002175 (2011).
444 14. Lipsitch, M.*, et al.* Are Anticapsular Antibodies the Primary Mechanism of Protection against Invasive
445 Pneumococcal Disease? *PLoS Med* **2**, e15 (2005).
446 15. Ratner, A.J.*, et al.* Epithelial cells are sensitive detectors of bacterial pore-forming toxins. *J Biol Chem*
447 **281**, 12994-12998 (2006).
448 16. Ratner, A.J., Lysenko, E.S., Paul, M.N. & Weiser, J.N. Synergistic proinflammatory responses induced
449 by polymicrobial colonization of epithelial surfaces. *Proc Natl Acad Sci U S A* **102**, 3429-3434 (2005).
450 17. Eisele, N.A. & Anderson, D.M. Host Defense and the Airway Epithelium: Frontline Responses That
451 Protect against Bacterial Invasion and Pneumonia. *J Pathog* **2011**, 249802 (2011).
452 18. Ganesan, S., Comstock, A.T. & Sajjan, U.S. Barrier function of airway tract epithelium. *Tissue Barriers*
453 **1**, e24997 (2013).
454 19. Whitsett, J.A. & Alenghat, T. Respiratory epithelial cells orchestrate pulmonary innate immunity. *Nat*
455 *Immunol* **16**, 27-35 (2015).
456 20. Wilson, R.*, et al.* Protection against Streptococcus pneumoniae lung infection after nasopharyngeal
457 colonization requires both humoral and cellular immune responses. *Mucosal Immunol* **8**, 627-639
458 (2015).
459 21. Clarke, T.B., Francella, N., Huegel, A. & Weiser, J.N. Invasive bacterial pathogens exploit TLR-
460 mediated downregulation of tight junction components to facilitate translocation across the
461 epithelium. *Cell Host Microbe* **9**, 404-414 (2011).
462 22. Weiser, J.N., Ferreira, D.M. & Paton, J.C. Streptococcus pneumoniae: transmission, colonization and
463 invasion. *Nat Rev Microbiol* **16**, 355-367 (2018).

464 23. Agarwal, V., Asmat, T.M., Dierdorf, N.I., Hauck, C.R. & Hammerschmidt, S. Polymeric immunoglobulin
465 receptor-mediated invasion of Streptococcus pneumoniae into host cells requires a coordinate
466 signaling of SRC family of protein-tyrosine kinases, ERK, and c-Jun N-terminal kinase. *J Biol Chem* **285**,
467 35615-35623 (2010).
468 24. Asmat, T.M., Agarwal, V., Saleh, M. & Hammerschmidt, S. Endocytosis of Streptococcus pneumoniae
469 via the polymeric immunoglobulin receptor of epithelial cells relies on clathrin and caveolin
470 dependent mechanisms. *Int J Med Microbiol* **304**, 1233-1246 (2014).
471 25. Beisswenger, C., Coyne, C.B., Shchepetov, M. & Weiser, J.N. Role of p38 MAP kinase and transforming
472 growth factor-beta signaling in transepithelial migration of invasive bacterial pathogens. *J Biol Chem*
473 **282**, 28700-28708 (2007).
474 26. Tomlinson, G.*, et al.* TLR-mediated inflammatory responses to Streptococcus pneumoniae are highly
475 dependent on surface expression of bacterial lipoproteins. *J Immunol* **193**, 3736-3745 (2014).
476 27. Ratner, A.J., Aguilar, J.L., Shchepetov, M., Lysenko, E.S. & Weiser, J.N. Nod1 mediates cytoplasmic
477 sensing of combinations of extracellular bacteria. *Cell Microbiol* **9**, 1343-1351 (2007).
478 28. Malley, R.*, et al.* Recognition of pneumolysin by Toll-like receptor 4 confers resistance to
479 pneumococcal infection. *Proc Natl Acad Sci U S A* **100**, 1966-1971 (2003).
480 29. Zafar, M.A., Wang, Y., Hamaguchi, S. & Weiser, J.N. Host-to-Host Transmission of Streptococcus
481 pneumoniae Is Driven by Its Inflammatory Toxin, Pneumolysin. *Cell Host Microbe* **21**, 73-83 (2017).
482 30. Matthias, K.A., Roche, A.M., Standish, A.J., Shchepetov, M. & Weiser, J.N. Neutrophil-toxin
483 interactions promote antigen delivery and mucosal clearance of Streptococcus pneumoniae. *J*
484 *Immunol* **180**, 6246-6254 (2008).
485 31. Ferreira, D.M.*, et al.* Controlled human infection and rechallenge with Streptococcus pneumoniae
486 reveals the protective efficacy of carriage in healthy adults. *Am J Respir Crit Care Med* **187**, 855-864
487 (2013).
488 32. Wright, A.K.*, et al.* Human nasal challenge with Streptococcus pneumoniae is immunising in the
489 absence of carriage. *PLoS Pathog* **8**, e1002622 (2012).
490 33. Pham, T.A.*, et al.* Epithelial IL-22RA1-mediated fucosylation promotes intestinal colonization
491 resistance to an opportunistic pathogen. *Cell Host Microbe* **16**, 504-516 (2014).
492 34. Zheng, M.*, et al.* Therapeutic Role of Interleukin 22 in Experimental Intra-abdominal Klebsiella
493 pneumoniae Infection in Mice. *Infect Immun* **84**, 782-789 (2016).
494 35. Van Maele, L.*, et al.* Activation of Type 3 innate lymphoid cells and interleukin 22 secretion in the
495 lungs during Streptococcus pneumoniae infection. *J Infect Dis* **210**, 493-503 (2014).
496 36. Trevejo-Nunez, G., Elsegeiny, W., Conboy, P., Chen, K. & Kolls, J.K. Critical Role of IL-22/IL22-RA1
497 Signaling in Pneumococcal Pneumonia. *J Immunol* **197**, 1877-1883 (2016).
498 37. Fais, S.*, et al.* HLA-DR antigens on colonic epithelial cells in inflammatory bowel disease: I. Relation
499 to the state of activation of lamina propria lymphocytes and to the epithelial expression of other
500 surface markers. *Clin Exp Immunol* **68**, 605-612 (1987).
501 38. Propst, S.M., Denson, R., Rothstein, E., Estell, K. & Schwiebert, L.M. Proinflammatory and Th2-derived
502 cytokines modulate CD40-mediated expression of inflammatory mediators in airway epithelia:
503 implications for the role of epithelial CD40 in airway inflammation. *J Immunol* **165**, 2214-2221 (2000).
504 39. Dugger, K., Lowder, T.W., Tucker, T.A. & Schwiebert, L.M. Epithelial cells as immune effector cells:
505 the role of CD40. *Semin Immunol* **21**, 289-292 (2009).
506 40. Cagnoni, F.*, et al.* CD40 on adult human airway epithelial cells: expression and proinflammatory
507 effects. *J Immunol* **172**, 3205-3214 (2004).
508 41. Huang, G.T., Eckmann, L., Savidge, T.C. & Kagnoff, M.F. Infection of human intestinal epithelial cells
509 with invasive bacteria upregulates apical intercellular adhesion molecule-1 (ICAM)-1) expression and
510 neutrophil adhesion. *J Clin Invest* **98**, 572-583 (1996).
511 42. Frick, A.G.*, et al.* Haemophilus influenzae stimulates ICAM-1 expression on respiratory epithelial cells.
512 *J Immunol* **164**, 4185-4196 (2000).
513 43. Tettelin, H.*, et al.* Complete genome sequence of a virulent isolate of Streptococcus pneumoniae.
514 *Science* **293**, 498-506 (2001).

515 44. Asmat, T.M., Agarwal, V., Rath, S., Hildebrandt, J.P. & Hammerschmidt, S. Streptococcus pneumoniae
516 infection of host epithelial cells via polymeric immunoglobulin receptor transiently induces calcium
517 release from intracellular stores. *J Biol Chem* **286**, 17861-17869 (2011).
518 45. Peter, A.*, et al.* Localization and pneumococcal alteration of junction proteins in the human alveolar-
519 capillary compartment. *Histochem Cell Biol* **147**, 707-719 (2017).
520 46. Malley, R.*, et al.* Recognition of pneumolysin by Toll-like receptor 4 confers resistance to
521 pneumococcal infection. *Proc Natl Acad Sci U S A* **100**, 1966-1971 (2003).
522 47. Herta, T.*, et al.* DNA-release by Streptococcus pneumoniae autolysin LytA induced Krueppel-like
523 factor 4 expression in macrophages. *Sci Rep* **8**, 5723 (2018).
524 48. Byng-Maddick, R.*, et al.* Tumor Necrosis Factor (TNF) Bioactivity at the Site of an Acute Cell-Mediated
525 Immune Response Is Preserved in Rheumatoid Arthritis Patients Responding to Anti-TNF Therapy.
526 *Front Immunol* **8**, 932 (2017).
527 49. Bell, L.C.*, et al.* In Vivo Molecular Dissection of the Effects of HIV-1 in Active Tuberculosis. *PLoS Pathog*
528 **12**, e1005469 (2016).
529 50. Pollara, G.*, et al.* Validation of Immune Cell Modules in Multicellular Transcriptomic Data. *PLoS One*
530 **12**, e0169271 (2017).
531 51. Siegel, S.J. & Weiser, J.N. Mechanisms of Bacterial Colonization of the Respiratory Tract. *Annu Rev*
532 *Microbiol* **69**, 425-444 (2015).
533 52. Mahdi, L.K., Ogunniyi, A.D., LeMessurier, K.S. & Paton, J.C. Pneumococcal virulence gene expression
534 and host cytokine profiles during pathogenesis of invasive disease. *Infect Immun* **76**, 646-657 (2008).
535 53. Briles, D.E., Novak, L., Hotomi, M., van Ginkel, F.W. & King, J. Nasal colonization with Streptococcus
536 pneumoniae includes subpopulations of surface and invasive pneumococci. *Infect Immun* **73**, 6945-
537 6951 (2005).
538 54. Morpeth, S.C.*, et al.* Detection of Pneumococcal DNA in Blood by Polymerase Chain Reaction for
539 Diagnosing Pneumococcal Pneumonia in Young Children From Low- and Middle-Income Countries.
540 *Clin Infect Dis* **64**, S347-S356 (2017).
541 55. Short, K.R.*, et al.* Influenza virus damages the alveolar barrier by disrupting epithelial cell tight
542 junctions. *Eur Respir J* **47**, 954-966 (2016).
543 56. Bootsma, H.J., Egmont-Petersen, M. & Hermans, P.W. Analysis of the in vitro transcriptional response
544 of human pharyngeal epithelial cells to adherent Streptococcus pneumoniae: evidence for a distinct
545 response to encapsulated strains. *Infect Immun* **75**, 5489-5499 (2007).
546 57. Gewirtz, A.T., Navas, T.A., Lyons, S., Godowski, P.J. & Madara, J.L. Cutting edge: bacterial flagellin
547 activates basolaterally expressed TLR5 to induce epithelial proinflammatory gene expression. *J*
548 *Immunol* **167**, 1882-1885 (2001).
549 58. Gewirtz, A.T.*, et al.* Salmonella typhimurium translocates flagellin across intestinal epithelia, inducing
550 a proinflammatory response. *J Clin Invest* **107**, 99-109 (2001).
551 59. Hornef, M.W., Wick, M.J., Rhen, M. & Normark, S. Bacterial strategies for overcoming host innate
552 and adaptive immune responses. *Nat Immunol* **3**, 1033-1040 (2002).
553 60. Zanin, M., Baviskar, P., Webster, R. & Webby, R. The Interaction between Respiratory Pathogens and
554 Mucus. *Cell Host Microbe* **19**, 159-168 (2016).
555 61. Vareille, M., Kieninger, E., Edwards, M.R. & Regamey, N. The airway epithelium: soldier in the fight
556 against respiratory viruses. *Clin Microbiol Rev* **24**, 210-229 (2011).
557 62. Koppe, U.*, et al.* Streptococcus pneumoniae stimulates a STING- and IFN regulatory factor 3-
558 dependent type I IFN production in macrophages, which regulates RANTES production in
559 macrophages, cocultured alveolar epithelial cells, and mouse lungs. *J Immunol* **188**, 811-817 (2012).
560 63. Zafar, M.A., Kono, M., Wang, Y., Zangari, T. & Weiser, J.N. Infant Mouse Model for the Study of
561 Shedding and Transmission during Streptococcus pneumoniae Monoinfection. *Infect Immun* **84**,
562 2714-2722 (2016).
563 64. Plotkowski, M.C., Puchelle, E., Beck, G., Jacquot, J. & Hannoun, C. Adherence of type I Streptococcus
564 pneumoniae to tracheal epithelium of mice infected with influenza A/PR8 virus. *Am Rev Respir Dis*
565 **134**, 1040-1044 (1986).

566 65. Pittet, L.A., Hall-Stoodley, L., Rutkowski, M.R. & Harmsen, A.G. Influenza virus infection decreases
567 tracheal mucociliary velocity and clearance of Streptococcus pneumoniae. *Am J Respir Cell Mol Biol*
568 **42**, 450-460 (2010).
569 66. McCullers, J.A., Iverson, A.R., McKeon, R. & Murray, P.J. The platelet activating factor receptor is not
570 required for exacerbation of bacterial pneumonia following influenza. *Scand J Infect Dis* **40**, 11-17
571 (2008).
572 67. Zahlten, J.*, et al.* Role of Pneumococcal Autolysin for KLF4 Expression and Chemokine Secretion in
573 Lung Epithelium. *Am J Respir Cell Mol Biol* **53**, 544-554 (2015).
574 68. Zahlten, J.*, et al.* TLR9- and Src-dependent expression of Krueppel-like factor 4 controls interleukin-
575 10 expression in pneumonia. *Eur Respir J* **41**, 384-391 (2013).
576 69. Hotomi, M., Yuasa, J., Briles, D.E. & Yamanaka, N. Pneumolysin plays a key role at the initial step of
577 establishing pneumococcal nasal colonization. *Folia Microbiol (Praha)* **61**, 375-383 (2016).
578 70. Parker, D.*, et al.* Streptococcus pneumoniae DNA initiates type I interferon signaling in the respiratory
579 tract. *MBio* **2**, e00016-00011 (2011).
580 71. Novick, S.*, et al.* Adhesion and invasion of Streptococcus pneumoniae to primary and secondary
581 respiratory epithelial cells. *Mol Med Rep* **15**, 65-74 (2017).
582 72. Glennie, S.J., Williams, N.A. & Heyderman, R.S. Mucosal immunity in resource-limited setting: is the
583 battle ground different? *Trends Microbiol* **18**, 487-493 (2010).
584 73. Browall, S.*, et al.* Intraclonal variations among Streptococcus pneumoniae isolates influence the
585 likelihood of invasive disease in children. *J Infect Dis* **209**, 377-388 (2014).
586 74. McCool, T.L., Cate, T.R., Moy, G. & Weiser, J.N. The immune response to pneumococcal proteins
587 during experimental human carriage. *J Exp Med* **195**, 359-365 (2002).
588 75. Hyams, C., Camberlein, E., Cohen, J.M., Bax, K. & Brown, J.S. The Streptococcus pneumoniae capsule
589 inhibits complement activity and neutrophil phagocytosis by multiple mechanisms. *Infect Immun* **78**,
590 704-715 (2010).
591 76. Collins, A.M.*, et al.* First human challenge testing of a pneumococcal vaccine. Double-blind
592 randomized controlled trial. *Am J Respir Crit Care Med* **192**, 853-858 (2015).
593 77. Jochems, S.P.*, et al.* Novel Analysis of Immune Cells from Nasal Microbiopsy Demonstrates Reliable,
594 Reproducible Data for Immune Populations, and Superior Cytokine Detection Compared to Nasal
595 Wash. *PLoS One* **12**, e0169805 (2017).
596 78. Bray, N.L., Pimentel, H., Melsted, P. & Pachter, L. Near-optimal probabilistic RNA-seq quantification.
597 *Nat Biotechnol* **34**, 525-527 (2016).
598 79. Soneson, C., Love, M.I. & Robinson, M.D. Differential analyses for RNA-seq: transcript-level estimates
599 improve gene-level inferences. *F1000Res* **4**, 1521 (2015).
600 80. Varet, H., Brillet-Gueguen, L., Coppee, J.Y. & Dillies, M.A. SARTools: A DESeq2- and EdgeR-Based R
601 Pipeline for Comprehensive Differential Analysis of RNA-Seq Data. *PLoS One* **11**, e0157022 (2016).
602 81. Chakraborty, S., Datta, S. & Datta, S. Surrogate variable analysis using partial least squares (SVA-PLS)
603 in gene expression studies. *Bioinformatics* **28**, 799-806 (2012).
604 82. Fang, H., Knezevic, B., Burnham, K.L. & Knight, J.C. XGR software for enhanced interpretation of
605 genomic summary data, illustrated by application to immunological traits. *Genome Med* **8**, 129
606 (2016).
607
608
609
610
611
612
613
614
615
616

617 **METHODS**

618

619 **Bacteria**

620 *S. pneumoniae* clinical strains used were 6B (BHN 418[73]), 23F (P1121[74]) and TIGR4 (P1672[75]),
621 together with a pneumolysin deficient TIGR4 mutant strain (kind gift from Prof T Mitchell, University
622 of Birmingham). Stocks of bacterial aliquots grown to $O.D._{600nm}$ 0.3 were stored at -80°C, defrosted,
623 resuspended in cell culture media and used once. Colony forming units (CFU) were counted on
624 horse blood agar plates (EO Labs).

625

626 **Experimental Human Pneumococcal Carriage Model (EHPC)**

627 Following written informed consent, healthy non-smoking adults between the ages of 18 – 59 were
628 inoculated with 80,000 CFU/nostril live 6B *S. pneumoniae* (BHN418), grown to mid-log phase in
629 vegetone broth as previously described[76]. Individuals naturally colonised with *S. pneumoniae* or in
630 regular contact with at-risk individuals were excluded. Nasal washes and mucosal cells (curette
631 biopsy) from the inferior turbinate were obtained by PBS syringe and curettage using a plastic Rhino-
632 probe™ (Arlington Scientific), in this order of collection respectively, before pneumococcal
633 inoculation. Sampling was then repeated on days 2, 6, 9, and 14 - 27 post pneumococcal
634 inoculation[77]. Volunteers received the TIV vaccine intramuscularly at day 3 post pneumococcal
635 inoculation. Bacteria collected from nasal washes were quantified by CFU counts. At each time-
636 point, two curettage samples were obtained and processed for confocal immunofluorescence, flow
637 cytometry, primary cell culture and /or transcriptomic analysis by RNA sequencing (RNAseq). There
638 were no adverse events. The carriage status of each volunteer was blinded until sample analysis
639 was completed.

640 Ethical approval was given by NHS Research and Ethics Committee (REC)/Liverpool School of
641 Tropical Medicine (LSTM) REC, reference numbers: 15/NW/0146 and 14/NW/1460 and Human
642 Tissue Authority licensing number 12548.

643

644 **Human Respiratory Tract Epithelial Cell Lines**

645 Human pharyngeal carcinoma Detroit 562 epithelial cells (ATCC_CCL-138) and human bronchial
646 carcinoma Calu3 epithelial cells (ATCC_HTB-55) were grown in 10% FCS in alpha MEM media
647 (Gibco). Human alveolar epithelial carcinoma A549 epithelial cells (ATCC_CCL-185) were grown in
648 10% FCS with 1% L-glutamine in Hams/F-12 media (Gibco).

649

650 **Pneumococcal-epithelial cell co-culture**

651 *Association and Invasion assays* - confluent Detroit 562 (typically day 8 post plating), Calu3 (typically
652 day 10 post plating) and A549 (typically day 4 post plating) monolayers cultured on 12 well plates
653 (Corning), were exposed to *S. pneumoniae* for three hours in 1% FCS alpha MEM. The medium was
654 removed and cells washed three times in $HBSS^{+/+}$. Cells were incubated in 1% saponin for 10
655 minutes at 37°C and lysed by repetitive pipetting. Dilutions of bacteria were plated on blood agar
656 and colonies counted after 16 hours. To quantify internalised bacteria, 100µg/ml gentamicin was
657 added for 1 hour to the cells, which were then washed another three times, before incubating with
658 1% Saponin and plating on blood agar plates. CFUs were counted after 16 hours incubation at 37°C,
659 5% CO_2. There were no differences in pneumococcal pre- or post-inoculum, or growth density
660 between the strains, in the cell supernatant three hours post-infection.

661

662 *Transmigration assay* - Detroit 562 cells were cultured on 3µm pore, PET Transwell Inserts
663 (ThermoFisher) typically for 10 days to achieve confluent, polarised monolayers. Calu3 cells were
664 plated onto Transwell inserts typically for 12 days and A549 cells typically for 6 days. Cell culture
665 media was changed 1 hour prior to addition of bacteria to 1% FCS (250µl apical chamber, 1ml basal
666 chamber). Resistance was recorded before and after *S. pneumoniae* were added using an EVOM2
667 (World Precision Instruments). 1mg/ml FITC-dextran (Sigma Aldrich) was added to the apical
668 chamber of selected inserts to assess permeability. Approximately 12 million bacteria were added
669 to the cells (~MOI 1 cell : 25 bacteria). During the time course, 50µl was removed, diluted and plated,
670 from the basal chamber to measure bacterial load by counting CFU/well. Permeability was recorded
671 using a FLUOstar Omega (BMG Labtech) at 488nm.

672

673 *Endocytosis inhibition assays* - Detroit 562 cells cultured on 12 well plates were treated with 100μM
674 dynasore (Cambridge Biosciences) and 7.5μg/ml nystatin (Sigma Aldrich) to block endocytosis for
675 30 minutes prior to, and for the duration of pneumococcal infection incubation period. DMSO was
676 used as a control. Cells were washed and treated with gentamicin and lysed with saponin as
677 described above.
678
679 **Confocal Microscopy**
680 For the *in vivo* analysis, mucosal cells derived by curettage from the EHPC model were placed
681 directly into 4% PFA for 1 hour. Cells were cytospun onto microscope slides and allowed to air dry.
682 For the *in vitro* analysis, epithelial cell lines on transwell membranes were fixed in either 4% PFA
683 (Pierce, Methanol Free) or 1:1 mix of methanol:acetone for 20 minutes. Cells were permeabilised
684 with 0.2% Triton X-100 for 10 minutes and blocked for 1 hour in blocking buffer (3% goat serum and
685 3% BSA in PBS) before incubation with anti-6B pneumococcal antisera, JAM-A, Claudin-4 or β-
686 catenin primary antibodies (see Supplementary Information) for one hour and then secondary and/or
687 conjugated antibodies for 45 minutes. DAPI solution was added for 5 minutes. After washing, the
688 stained samples were mounted using Aqua PolyMount (VWR International) with a coverslip onto a
689 microslide. The entire cytospin for each sample was manually viewed by microscopy for detection of
690 pneumococci. Multiple fields of view (>3) were imaged for each transwell insert, for each condition.
691 Images were captured using either an inverted LSM 700, LSM 880, or TissueFAXS Zeiss Confocal
692 Microscope. Z stacks were recorded at 1μm intervals at either 40x oil or 63x oil objectives. For the
693 *in vivo* samples, the operator (CMW) was blinded to the colonisation status of the volunteer at the
694 time of sampling.
695
696
697 **Flow cytometry**
698 For the *in vivo* analysis, cells from two curette samples were incubated in cold PBS++ (PBS
699 supplemented with 5mM EDTA and 0.5% FCS) were dislodged by pipetting and centrifuged at 440g
700 for 5 mins at 4°C. Supernatant was removed and cells resuspended in 25μl of PBS++ with
701 Live/Dead™ Fixable Violet Dead Cell Stain (ThermoFisher). After 15 minutes incubation on ice, an

702 antibody cocktail to stain for epithelial surface marker expression (see Supplementary Information)
703 was added and incubated for another 15 minutes. Samples were vortexed, resuspended in 3.5mls
704 of PBS++ and filtered over a pre-wetted 70µm filter. Samples were transferred to a 5ml FACS tube,
705 centrifuged and resuspended in 200µl Cell Fix (BD Biosciences) and acquired on LSRII Flow
706 Cytometer (BD Biosciences). Compensation was run and applied for each experimental replicate
707 and voltages consistent throughout. Isotype controls (Biolegend) and FL-1 controls were also run for
708 each antibody. Analyses of data was performed using FlowJo LLC version 10 software. Data was
709 performed on the gated epithelial cell population and only samples containing 500 or more cells are
710 reported.
711
712 For the *in vitro* analysis, confluent monolayers of Detroit 562 cells on 6 well plates were incubated
713 with *S. pneumoniae* for 6 hours in 1% FCS phenol free alpha MEM (base media, Life Technologies).
714 Cells were washed three times in PBS and gently lifted from the plate using a cell scraper in 300µl
715 of base media supplemented with 1mM EDTA. Samples were transferred to 5ml FACS tubes and
716 placed on ice for the duration of the protocol. Each cell sample was incubated with an antibody
717 cocktail for epithelial surface marker expression (see Supplemental Information) for 30 minutes
718 before rinsing in 1ml base media and centrifuging at 300g for 5 minutes at 4°C. Cells were fixed in
719 600µl of 4% PFA and acquired on a LSR II Flow Cytometer (BD Biosciences). Compensation was
720 run and applied for each experimental replicate and voltages consistent throughout. Isotype controls
721 (BD Biosciences), FL-1 and single stains were also run for each experiment. Samples were acquired
722 until 300,000 events had been collected. Analyses were performed using FlowJo LLC version 10
723 software.
724
725
726 **ELISAs**
727 Supernatant from Detroit 562 cells that had been incubated with *S. pneumoniae* for 6 hours, was
728 collected for cytokine analysis. IL-1β, IL-6, IL-8, IFNγ, TNFα, ICAM-1 DuoSet® ELISA kits were
729 purchased from R&D Systems and protocol followed according to manufacturers' instructions.
730

731 **RNA samples and sequencing (RNASeq)**

732 Mucosal curettage samples and epithelial cell cultures (incubated with or without *S. pneumoniae* for
733 3 hours) were collected in RNALater (ThermoFisher) and stored at -80°C. RNA Extraction was
734 performed using the RNEasy micro kit (Qiagen) and genomic DNA was removed with on column
735 DNA digestion or with the Turbo DNA-free Kit (Qiagen). Extracted RNA quality was assessed and
736 quantified using a BioAnalyser (Agilent 2100). Library preparation and RNA-sequencing (Illumina
737 Hiseq4000, 20M reads, 100 paired-end reads) were performed at the Beijing Genome Institute
738 (China) or the Sanger Institute (UK) for mucosal curettage samples. For the Detroit 562 samples,
739 library preparation was performed using the Kappa Hyperprep kit (Roche Diagnostics) and
740 sequencing was performed by the Pathogens Genomic Unit (UCL) on the Illumina Nextseq using
741 the Nextseq 500/550 High Output 75 cycle kit (Illumina) according to manufacturers' instructions,
742 giving 15-20 million 41bp paired end reads per sample.

743

744 All data processing and analysis was conducted in R, language and environment for statistical
745 computing (https://www.R-project.org). Paired end reads were mapped to the Ensembl human
746 transcriptome reference sequence (homo sapiens GRCh38). Mapping and generation of read counts
747 per transcript were performed using Kallisto[78], based on pseudoalignment. R/Bioconductor package
748 Tximport was used to import the mapped counts data and summarise the transcripts-level data into
749 gene level data[79]. DESeq2 and SARTools packages[80], were used for differential gene expression
750 analysis, using a false discovery rate (FDR) <0.05, following normalisation with a negative binomial
751 generalised linear model. In addition, transcript abundance for protein coding genes was expressed
752 as $\log_2$-transformed transcripts per million (TPM) by normalising the read counts to gene length and
753 then read depth. Transcriptomes from nasal samples ranged from 16 to 66 million reads per sample
754 and in principle component analysis, revealed a batch effect that was corrected by the Combat
755 function in the Surrogate Variable Analysis (SVA) R/Bioconductor package (Supplementary
756 Figure)[81].

757

758 Identification of interacting networks and pathway enrichment analysis was performed using XGR R
759 package[82]. Interacting genes (supported by at least one experimental source of evidence) were
760 identified from the Pathway Commons database for directed interactions (Supplementary File).
761 These were then subjected to Reactome pathway enrichment analysis with FDR<0.05
762 (Supplementary File). K-means clustering of Jaccard indices to quantify similarity between the
763 composition of genes mapping to each pathway was used to identify 20 groups of pathways, from
764 which the pathway consisting of the largest total number of genes was selected to provide a
765 representative annotation for each group. The expression of gene modules in the nasal
766 transcriptomes was represented by the mean Log_2 TPM value of the genes in each module.

767

768 **Statistics**

769 All experiments were conducted with replicates in three or more independent experiments unless
770 stated otherwise. Error bars represent SEM unless stated otherwise. GraphPad Prism Version 10
771 was used to perform two-tailed parametric (t-tests or ANOVA) or non-parametric (Mann-Whitney or
772 Kruskal-Wallis tests) analysis, which was based on the Shapiro-Wilk normality test. P values less
773 than 0.05 were considered significant and are derived from non-parametric statistical tests unless
774 stated otherwise.

775
776
777
778
779
780
781
782
783
784
785

786 **FIGURE LEGENDS**

787

788 **Table 1. *Streptococcus pneumoniae* association with the nasal epithelium in the EHPC model**
789 **detected by culture, confocal microscopy and LytA PCR**

790 Nasal washes and nasal curette biopsies were collected from carriage positive and carriage negative
791 volunteers over time. Standard methods for measuring bacterial density by culture (CFU) and LytA
792 PCR were compared against counts visualised by confocal microscopy for pneumococcal
793 association with nasal cells over time. The data was derived from 13 volunteers. + (1-10
794 pneumococci); ++ (11-50 pneumococci); +++ (51-100 pneumococci); ++++ (>100 pneumococci); n/a
795 = reading not taken.

796

797 **Figure 1. *Streptococcus pneumoniae* colonisation of the human nasal epithelium from the**
798 **EHPC model is associated with adhesion, microcolony formation and micro-invasion but**
799 **does not alter epithelial surface marker expression, in response to 6B colonisation**

800 (a) Representative fields from the EHPC model nasal curette biopsies show intact epithelium can be
801 obtained from the samples (as visualised by XY planes) and they retain their size and shape (as
802 visualised by XZ planes). Cells were stained with Wheat Germ Agglutinin (WGA) or Junctional
803 Adhesion Molecule -A (JAM-A, red) and nuclei. (b) The pattern of pneumococcal density detected
804 by culture and microscopy. (c) The proportion of bacteria located on the cell surface, intracellularly,
805 or paracellularly visualised by confocal microscopy, quantified from 8 volunteers collected over time
806 from microscopy counts. (d) Cells were stained for surface carbohydrates using WGA (red), and the
807 bacteria were marked with specific serotype antiserum (green). XY images of 1µm slices through a
808 layer of cells, with bacteria associated. (e) Examples of cells showing; (ei) Microcolony formation on
809 the surface of the epithelium, (eii) bacterial internalization, (eiii) migration through epithelial uptake
810 internally or between cells. (f) Co-association between *S. pneumoniae* (green) and JAM-A (red).
811 Nuclei (blue). Bacterial uptake appeared co-associated with JAM-A (yellow).

812 Epithelial cells from nasal curette biopsies were analysed by flow cytometry for (g) CD54 and (h)
813 CD107a. Results were expressed as median fluorescence intensity (left) and high cell surface
814 expression (≥95% of the baseline expression) representing at least two volunteers per time point
815 who were carriage negative (black) and carriage positive (grey).

816

817 **Figure 2. *Streptococcus pneumoniae* infection of nasopharyngeal epithelium *in vitro* is**
818 **associated with adhesion, microcolony formation, micro-invasion, transmigration and is**
819 **partially influenced by pneumolysin. Transmigration of *S. pneumoniae* is endocytosis-**
820 **dependent but does not disrupt barrier integrity or function**

821 (a) Pneumococcal association and (b) internalisation: ~$1x10^6$ Detroit 562 cell monolayers were
822 stimulated with ~$7x10^6$ pneumococci for 1 or 3 hours and the quantity of bacteria associated with the
823 cells was determined by culture (CFU); n>3. (****P = <0.0001: (a) 1hr (dashed lines) - ANOVA; 3hr
824 (solid lines) - Kruskall-Wallis; (b) Kruskall-Wallis). (c) Pneumococcal transmigration: ~$4.9x10^5$ cells
825 cultured on transwell inserts were stimulated with ~$1.2x10^7$ pneumococci for 3 hours and bacterial
826 density in the basal chamber was determined (**P = 0.0092, Kruskall-Wallis test). N = 5. (di)
827 Representative pneumococcal-density (green) images of cells (blue nuclei) after infection. Scale bar
828 = 20µm. n>3. (e - h) Representative images of pneumococcal localization (green) from cells (red,
829 JAM-A), illustrating: (e) differences in adherence by 6B and TIGR4; (f) internalised bacteria co-
830 localised with JAM-A with associated intracellular vesicle-like bodies (yellow); (g) lateral localisation
831 of pneumococci (XY images) with possible paracellular movement co-associated with JAM-A (XZ
832 images); (h) basal localisation of bacteria at the level of nuclei and insert pores. n = >20. (i and j)
833 Cells were treated with dynasore and nystatin for 30 minutes prior to and during incubation with 23F,
834 for 1 hour. (i) Intracellular bacteria were quantified and CFUs counted (****P = <0.0001, Mann-
835 Whitney Test). (j) Transmigrated bacteria after one hour were counted by CFUs (*P = 0.013 Mann-
836 Whitney Test). N = 4. (k and l) Cells were co-infected with pneumococci for three hours on transwell
837 inserts and barrier function recorded. (k) TEER was compared before and after exposure to
838 pneumococci. n = 9. Calcium withdrawal = positive control (***P = 0.0013, unpaired T-test). n = 3. (l)
839 Permeability was assessed by leak to 4kDa FITC-dextran, collected from the basal chamber. N =

840 >4. ****P = <0.0001 comparing non-infected against pneumococcal strains (Kruskall-Wallis test).
841 Blank inserts = positive control (Mann-Whitney test).

842

843 **Figure 3. Epithelial surface activation-marker expression and cytokine secretion is**
844 **upregulated after *S. pneumoniae* exposure**

845 (a and b) Detroit 562 cells were stimulated with *S. pneumoniae* for 6 hours and the median
846 fluorescence intensity and high-expressing cells for (a) CD54 and (b) CD107a were analysed by flow
847 cytometry. n = >3 independent experiments (**** P < 0.0001 CD107a MFI, compared to non-infected
848 cells, ANOVA. *** P = 0.0009 for MFI CD107a, TIGR4 v dPly, unpaired T-test. *** P < 0.001 CD107a
849 high expression, compared to non-infected cells, ANOVA *P = 0.028 for high expression CD107a,
850 TIGR4 vs. dPly, Mann-Whitney). (* P = 0.048 NI v TIGR4; * P = 0.0367 NI v dPly for CD54, ANOVA).

851 (c) IL-6, IL-8 and CD54 in the supernatants from Detroit 562 cells stimulated with *S. pneumoniae* for
852 6 hours, were measured by ELISA. N = 6 independent experiments with replicates. (**** P <0.0001
853 IL-6; *** P = 0.0013 CD54; **** P < 0.0001 IL-8 (Kruskall-Wallis test)).

854

855 **Figure 3. Transmigration of *S. pneumoniae* is endocytosis-dependent but does not**
856 **disrupt barrier integrity or function**

857 (a and b) Detroit 562 cells were treated with dynasore and nystatin for 30 minutes prior to and during
858 incubation with 23F, for 1 hour. (a) Intracellular bacteria were quantified using a gentamicin
859 protection assay and CFUs counted (**** P = <0.0001, Mann-Whitney Test). (b) Bacteria that had
860 transmigrated after one hour were then counted by CFUs (* P = 0.013 Mann-Whitney Test). N = 4
861 independent experiments with replicates. (c and d) Detroit 562 cells were co-infected with
862 pneumococci for three hours on transwell inserts and TEER and permeability were recorded. (c).
863 TEER was compared before and after exposure to pneumococci. n = 9 independent experiments
864 with replicates. Calcium withdrawal was used as a positive control *** P = 0.0013 (n = 3 with
865 replicates, unpaired T-test). (d) Permeability was assessed by leak to 4kDa FITC-dextran, collected

866 from the basal chamber. N = >4 independent experiments. **** P = <0.0001 comparing non-infected
867 against pneumococcal strains (Kruskall-Wallis test). Blank inserts were used as a positive control
868 (Mann-Whitney test).

869

870 **Figure 4. *Streptococcus pneumoniae* induces epithelial innate transcriptomic responses *in*
871 *vitro* that are influenced by the pattern of epithelial adhesion and micro-invasion**

872 (a) The total number of Detroit 562 epithelial genes upregulated following exposure to 6B, 23F,
873 TIGR4 and TIGR4-dPly pneumococci, compared to non-infected samples. N = 3 independent
874 experiments with replicates. Genes with an FDR <0.05 were considered for further analysis. The
875 matrix shows intersections for the four strains, sorted by size. Dark circles in the matrix indicates
876 sets that are part of the intersection. (b) Bubble heat map showing the results of Reactome Pathway
877 Analysis for upregulated genes in each strain compared to non-infected cells. Pathways were
878 clustered in 20 groups using K-means on Jaccard index and the biggest pathway for each group
879 was selected as representative of the group and visualised here. The colour represents the log2 z-
880 scores (a continuum from blue (lowest values) and red (highest values) and the size shows the
881 number of genes annotated to each pathway. (c) Selected bubble heat map clusters representing
882 the individual pathways within each cluster from 5b. (d) Bubble heat map showing the results of
883 transcriptional factor analysis in Opossum for each strain. Transcriptional factors are ordered by
884 family and then sorted by number of genes in the database. The colour represents the log2 z-scores
885 (a continuum from blue to red as before) and the size shows the number of genes annotated to the
886 particular pathway.

887

888 **Figure 5. Epithelial transcriptomic responses to *Streptococcus pneumoniae* in the EHPC
889 model**

890 (a) Network representation generated from the *in vitro* analyses for each strain. From the genes
891 present in the networks, an integrated gene list (200 genes) and a core genes list (16 genes) were
892 generated and tested as modules in the *in vivo* data. (b and c) Upregulated genes in comparison to

893 the transcriptomes of carriage negative and carriage positive volunteers were compared between
894 time points. Plots represent log2 TPM arithmetic mean for genes in the core (b) and integrated (c)
895 modules. P = <0.05, (one tail Mann-Whitney test). Number of samples for carriage negative and
896 positive, respectively: pre (17:14), day 2 (15:14), day 9 (7:7).
897

898 **Figure 6. Model of the control of pneumococcal colonisation by the human mucosal**
899 **epithelium.**

900 Following pneumococcal adhesion and microcolony formation on the epithelial surface, the
901 host response is dependent on the subsequent pattern of interaction. Microinvasion
902 (endocytosis and paracellular transmigration) amplifies epithelial sensing and inflammation/
903 innate immunity, which we postulate leads to immune cell engagement. This process of
904 epithelial sensing inflammation/ innate immunity may enhance both transmission and
905 clearance. Co-association with junctional proteins may facilitate migration across the barrier.

906

Table 1

		Sample day					Pneumococcal association		
ID	**Pneumococcal density**	**Pre**	**D2**	**D6**	**D9**	**D27**	**Surface**	**Intracellular**	**Lateral**
1	**Culture (CFU/ml)**	0	373	520	10	2			
	Microscopy (counts)	0	+	+	0	+	+	0	0
	LytA PCR	NEG	POS	POS	n/a	POS			
2	**Culture (CFU/ml)**	0	0	0	0	0			
	Microscopy (counts)	+	+	0	0	0	++	+	0
	LytA PCR	NEG	NEG	NEG	n/a	NEG			
3	**Culture (CFU/ml)**	0	0	0	0	0			
	Microscopy (counts)	0	+	0	0	0	+	0	0
	LytA PCR	NEG	POS	NEG	n/a	NEG			
4	**Culture (CFU/ml)**	0	3	9	0	0			
	Microscopy (counts)	0	0	0	+	0	+	0	0
	LytA PCR	NEG	POS	POS	n/a	NEG			
5	**Culture (CFU/ml)**	0	$7x10^3$	223	22	0			
	Microscopy (counts)	0	+	+	+	0	+	+	0
	LytA PCR	n/a	n/a	n/a	n/a	n/a			
6	**Culture (CFU/ml)**	0	$1.9x10^4$	$5.7x10^3$	$3.7x10^4$	11			
	Microscopy (counts)	0	++	++++	++	0	+++	++	+
	LytA PCR	NEG	POS	POS	n/a	POS			
7	**Culture (CFU/ml)**	0	822	$1.1x10^3$	160	0			
	Microscopy (counts)	0	+	+++	++	0	++	+	+
	LytA PCR	NEG	POS	POS	n/a	NEG			
8	**Culture (CFU/ml)**	0	0	0	0	0			
	Microscopy (counts)	0	0	0	0	0	0	0	0
	LytA PCR	n/a	n/a	n/a	n/a	n/a			
9	**Culture (CFU/ml)**	0	221	695	4	<1			
	Microscopy (counts)	n/a	+	+++	+	n/a	+++	+	+
	LytA PCR	NEG	POS	POS	n/a	NEG			
10	**Culture (CFU/ml)**	0	$1x10^3$	0	0	0			
	Microscopy (counts)	n/a	0	+	0	n/a	+	0	0
	LytA PCR	NEG	POS	POS	n/a	POS			
11	**Culture (CFU/ml)**	0	$1.8x10^6$	$1.8x10^6$	$1.9x10^4$	<1			
	Microscopy (counts)	n/a	++++	++++	+	n/a	+++	+	+
	LytA PCR	NEG	POS	POS	n/a	NEG			
12	**Culture (CFU/ml)**	0	0	0	0	0			
	Microscopy (counts)	NR	++	0	0	n/a	++	+	+
	LytA PCR	NEG	NEG	NEG	n/a	NEG			
13	**Culture (CFU/ml)**	0	23	2	0	0			
	Microscopy (counts)	n/a	+	0	0	n/a	+	0	0
	LytA PCR	POS	POS	POS	n/a	POS			

Figure 1

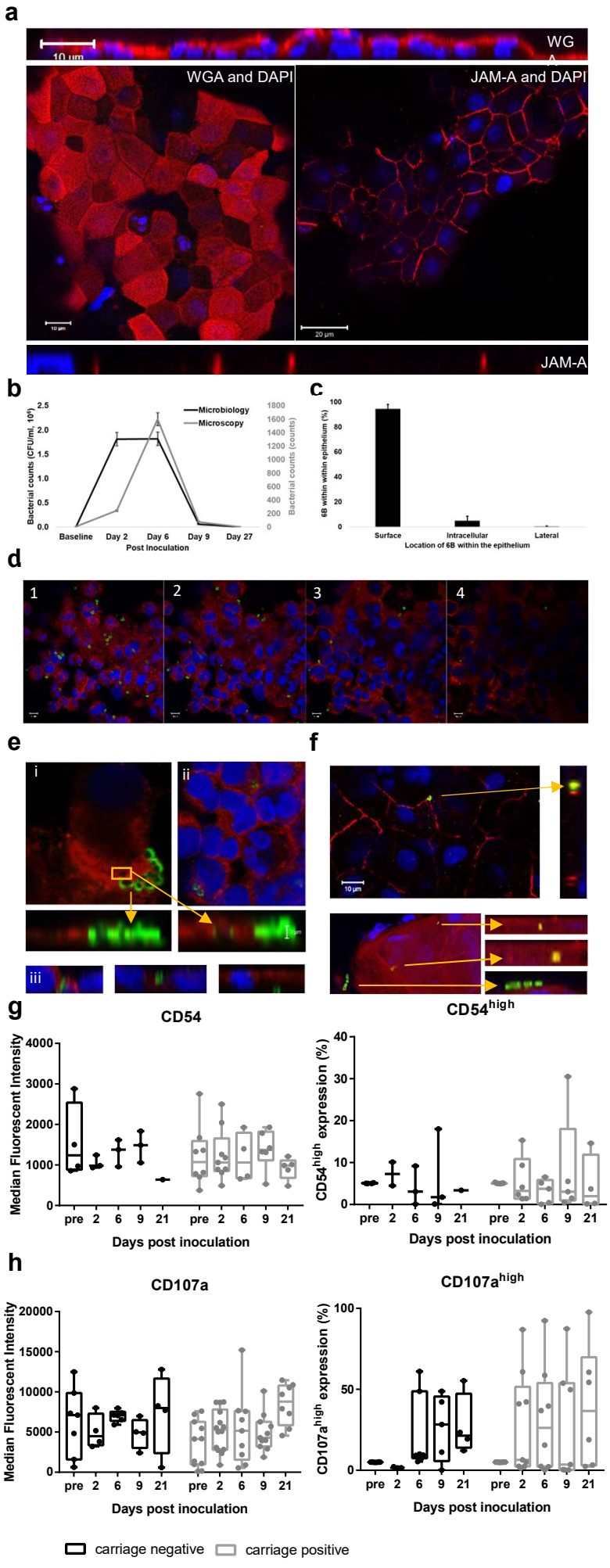
a
WG
WGA and DAPI
JAM-A and DAPI
JAM-A
b
Microbiology
Microscopy
Bacterial counts (CFU/ml, 10^6)
Bacterial counts (counts)
Baseline
Day 2
Day 6
Day 9
Day 27
Post inoculation
c
6B within within epithelium (%)
Surface
Intracellular
Lateral
Location of 6B within the epithelium
d
1
2
3
4
e
i
ii
iii
f
g
CD54
CD54high
Median Fluorescent Intensity
CD54high expression (%)
pre
Days post inoculation
h
CD107a
CD107ahigh
Median Fluorescent Intensity
CD107ahigh expression (%)
carriage negative
carriage positive

Figure 2

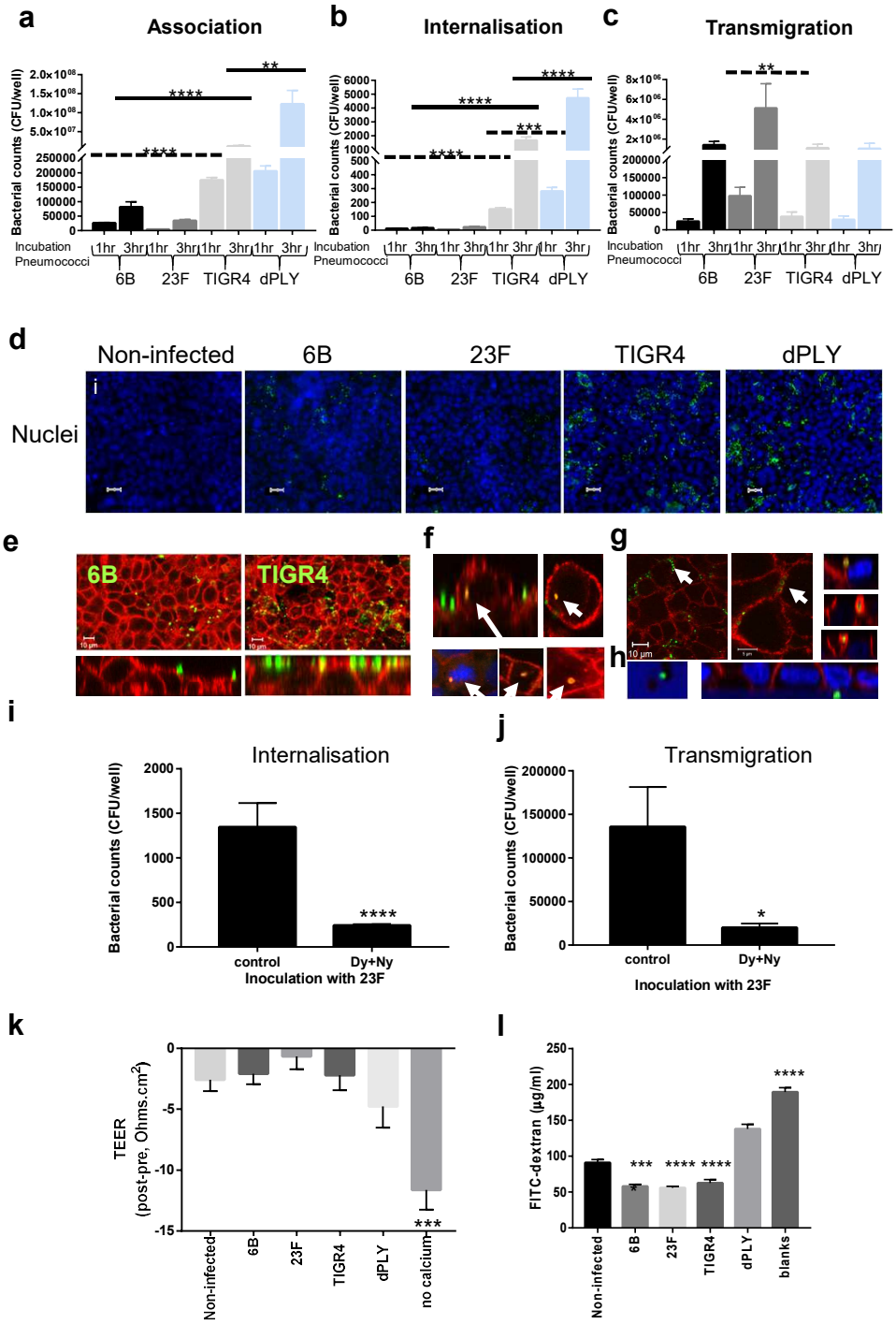
a
Association
b
Internalisation
c
Transmigration
Bacterial counts (CFU/well)
Incubation
Pneumococci
1hr 3hr 1hr 3hr 1hr 3hr 1hr 3hr
6B 23F TIGR4 dPLY
d
Non-infected
6B
23F
TIGR4
dPLY
Nuclei
e
6B
TIGR4
f
g
h
i
Internalisation
Bacterial counts (CFU/well)
control
Dy+Ny
Inoculation with 23F
j
Transmigration
Bacterial counts (CFU/well)
control
Dy+Ny
Inoculation with 23F
k
TEER
(post-pre, Ohms.cm2)
Non-infected
6B
23F
TIGR4
dPLY
no calcium
l
FITC-dextran (µg/ml)
Non-infected
6B
23F
TIGR4
dPLY
blanks

Figure 3

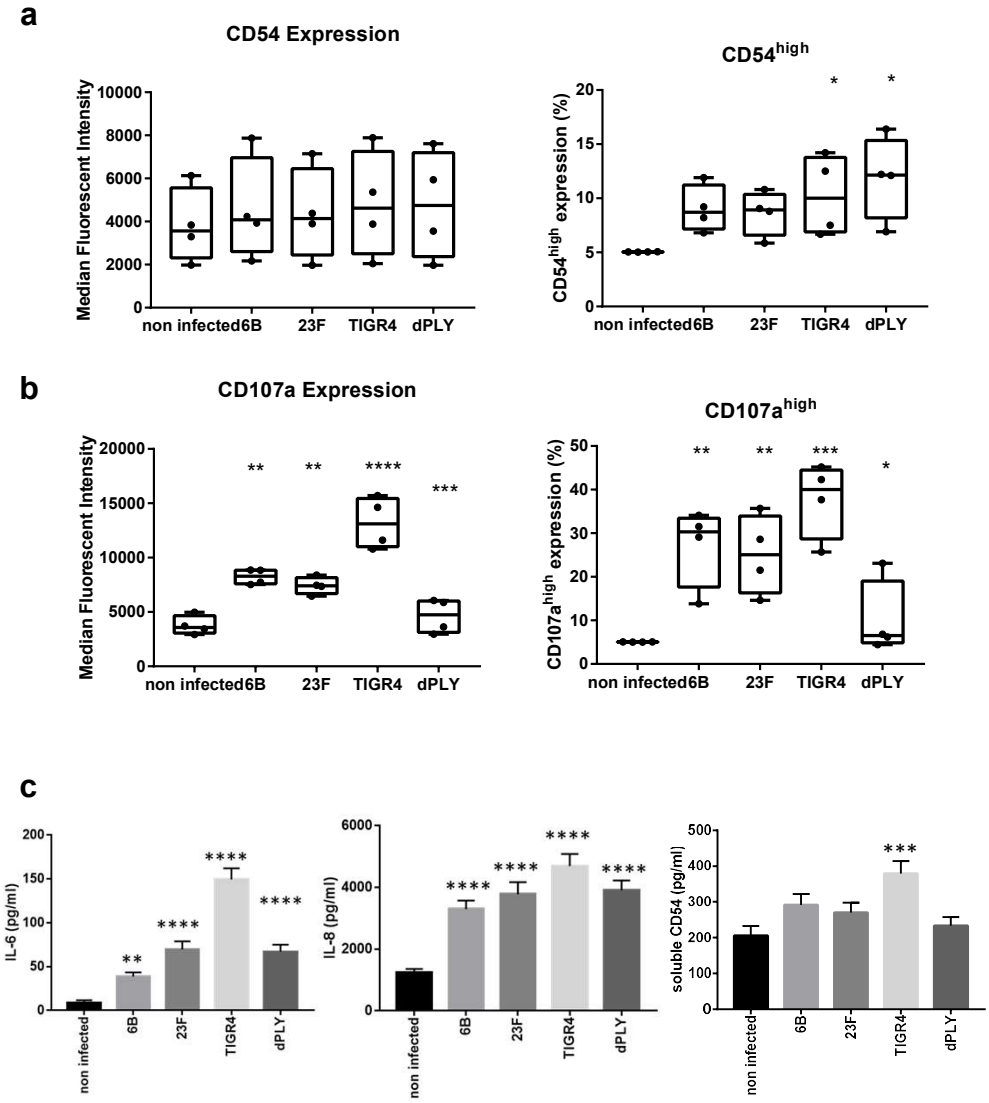
a
CD54 Expression
Median Fluorescent Intensity
10000
8000
6000
4000
2000
0
non infected
6B
23F
TIGR4
dPLY
CD54high
CD54high expression (%)
20
15
10
5
0
*
*
b
CD107a Expression
Median Fluorescent Intensity
20000
15000
10000
5000
0
**
**
****
***
CD107ahigh
CD107ahigh expression (%)
50
40
30
20
10
0
**
**
***
*
c
IL-6 (pg/ml)
200
150
100
50
0
**
****
****
****
non infected
6B
23F
TIGR4
dPLY
IL-8 (pg/ml)
6000
4000
2000
0
****
****
****
****
soluble CD54 (pg/ml)
500
400
300
200
100
0
***

Figure 4

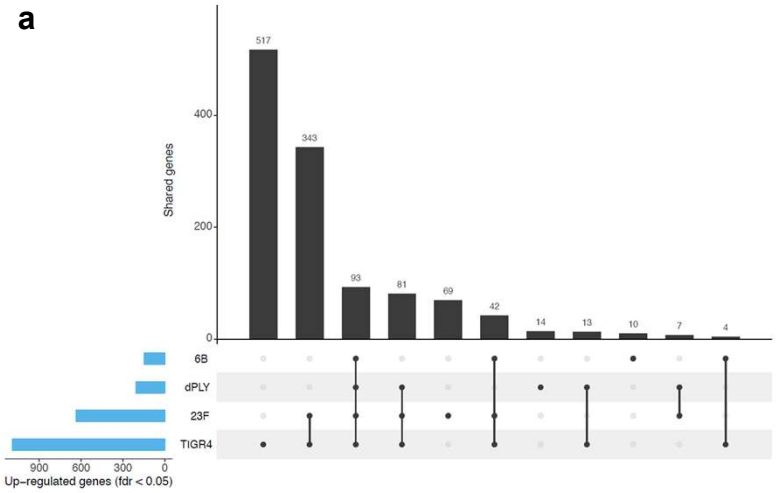
a
Shared genes
517
343
93
81
69
42
14
13
10
7
4
6B
dPLY
23F
TIGR4
Up-regulated genes (fdr < 0.05)

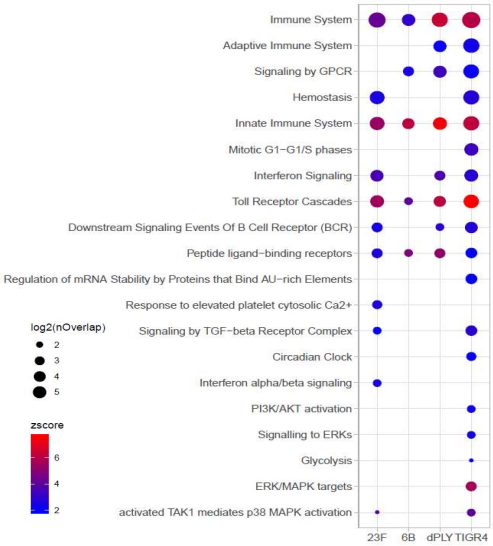
b
Immune System
Adaptive Immune System
Signaling by GPCR
Hemostasis
Innate Immune System
Mitotic G1-G1/S phases
Interferon Signaling
Toll Receptor Cascades
Downstream Signaling Events Of B Cell Receptor (BCR)
Peptide ligand-binding receptors
Regulation of mRNA Stability by Proteins that Bind AU-rich Elements
Response to elevated platelet cytosolic Ca2+
Signaling by TGF-beta Receptor Complex
Circadian Clock
Interferon alpha/beta signaling
PI3K/AKT activation
Signalling to ERKs
Glycolysis
ERK/MAPK targets
activated TAK1 mediates p38 MAPK activation
log2(nOverlap)
zscore
23F
6B
dPLY
TIGR4

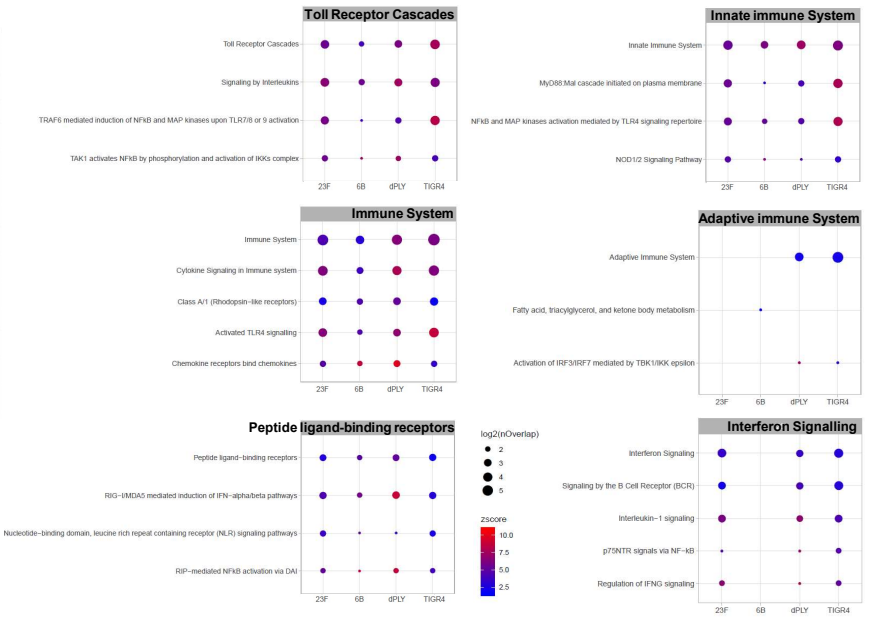
c
Toll Receptor Cascades
Toll Receptor Cascades
Signaling by Interleukins
TRAF6 mediated induction of NFkB and MAP kinases upon TLR7/8 or 9 activation
TAK1 activates NFkB by phosphorylation and activation of IKKs complex
Innate immune System
Innate Immune System
MyD88:Mal cascade initiated on plasma membrane
NFkB and MAP kinases activation mediated by TLR4 signaling repertoire
NOD1/2 Signaling Pathway
Immune System
Immune System
Cytokine Signaling in Immune system
Class A/1 (Rhodopsin-like receptors)
Activated TLR4 signalling
Chemokine receptors bind chemokines
Adaptive immune System
Adaptive Immune System
Fatty acid, triacylglycerol, and ketone body metabolism
Activation of IRF3/IRF7 mediated by TBK1/IKK epsilon
Peptide ligand-binding receptors
Peptide ligand-binding receptors
RIG-I/MDA5 mediated induction of IFN-alpha/beta pathways
Nucleotide-binding domain, leucine rich repeat containing receptor (NLR) signaling pathways
RIP-mediated NFkB activation via DAI
Interferon Signalling
Interferon Signaling
Signaling by the B Cell Receptor (BCR)
Interleukin-1 signaling
p75NTR signals via NF-kB
Regulation of IFNG signaling
log2(nOverlap)
zscore
23F
6B
dPLY
TIGR4

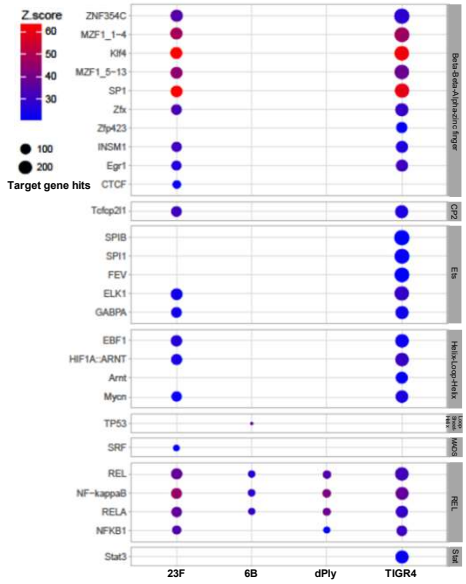
d
Z.score
Target gene hits
ZNF354C
MZF1_1-4
Klf4
MZF1_5-13
SP1
Zfx
Zfp423
INSM1
Egr1
CTCF
Tcfcp2l1
SPIB
SPI1
FEV
ELK1
GABPA
EBF1
HIF1A::ARNT
Arnt
Mycn
TP53
SRF
REL
NF-kappaB
RELA
NFKB1
Stat3
23F
6B
dPly
TIGR4

Figure 5

a

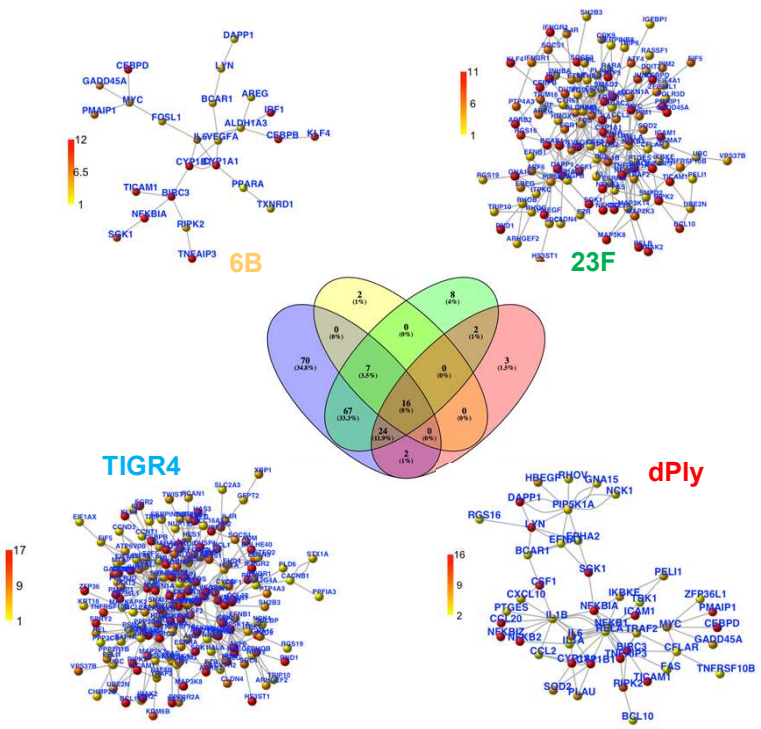
6B
23F
TIGR4
dPly

b

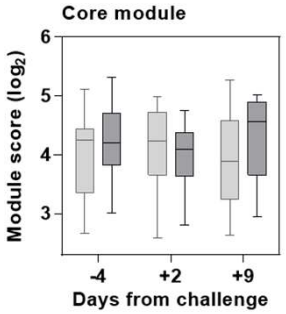
Core module
Module score (log2)
-4
+2
+9
Days from challenge

c

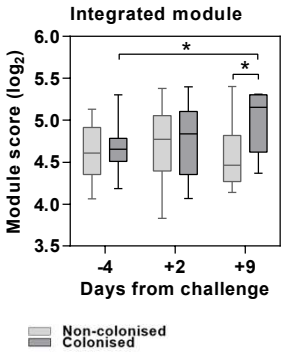
Integrated module
Module score (log2)
-4
+2
+9
Days from challenge
Non-colonised
Colonised

Figure 6

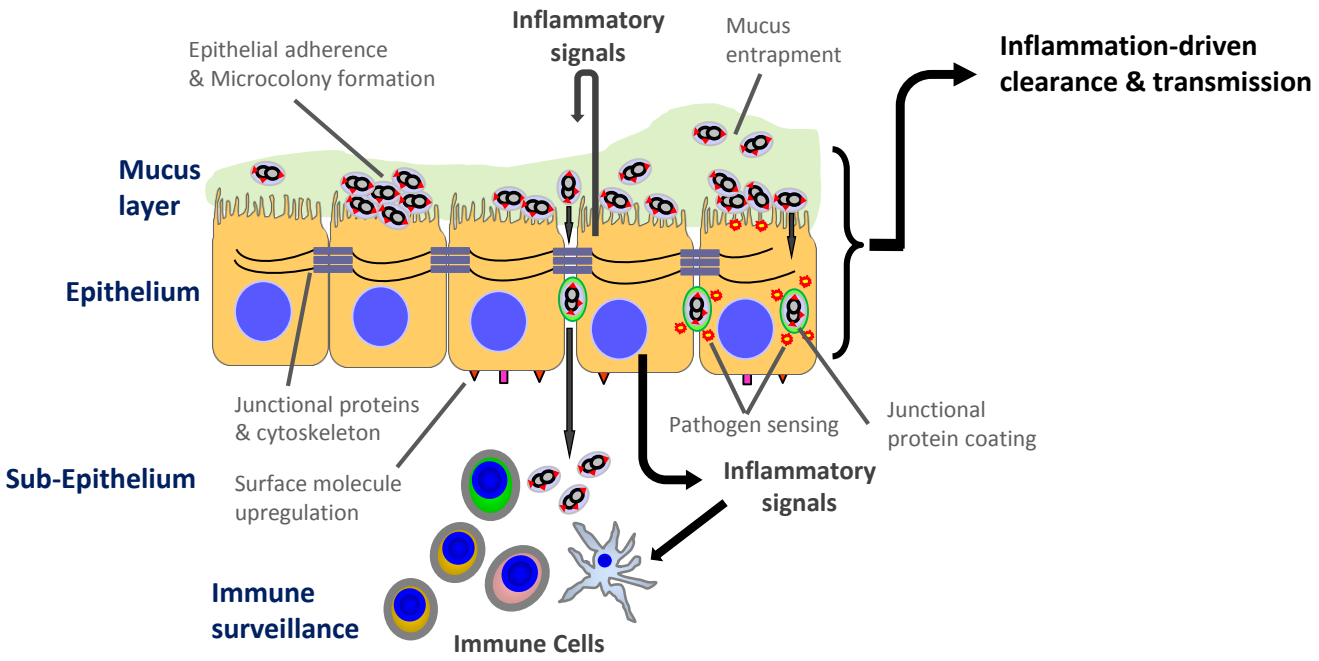
Inflammatory signals
Mucus entrapment
Epithelial adherence & Microcolony formation
Inflammation-driven clearance & transmission
Mucus layer
Epithelium
Junctional proteins & cytoskeleton
Pathogen sensing
Junctional protein coating
Sub-Epithelium
Surface molecule upregulation
Inflammatory signals
Immune surveillance
Immune Cells